FACTA UNIVERSITATIS
Series: **Architecture and Civil Engineering** Vol. 8, N° 1, 2010, pp. 1 - 12
DOI: 10.2298/FUACE1001001M

COMPUTATIONAL MODELLING OF FAILURE MECHANISMS IN REINFORCED CONCRETE STRUCTURES

UDC 624.012.45:539.56:519.711(045)=111

Peter Mark, Michél Bender

Institute of Concrete Structures, Faculty of Civil and Environmental Engineering,
Ruhr-University Bochum, 44780 Bochum, Germany
E-mail: peter.mark@rub.de, michel.bender@rub.de

Abstract. *A modelling approach for macroscopic reinforced concrete (RC) structures and structural elements under static loading conditions is presented. It uses the embedded modelling technique to separately account for concrete volumes and single longitudinal bars or stirrups. The material equations of the 3D elasto-plastic damage model for concrete are derived assuming isotropic damage, stiffness recovery and loss due to crack closing and reopening and a non-associated flow rule. Suitable material functions and material parameters as well as a regularisation by energy criteria are given. The approach is applied to shear beam tests illustrating numerical results compared to corresponding experimental data.*

Key words: *numerical simulation, reinforced concrete, concrete model, embedded modelling, damage evolution, shear failure, circular sections*

1. INTRODUCTION

Numerical simulations of reinforced concrete structures grow more and more in their variety of applications [1, 2]. They usually base on continuum damage theories [3, 4] and finite element methods [5, 6] modelling the effects of cracking in an indirect way by distributed reductions in stiffness parameters. The simulations often focus on

– overall nonlinear structural aspects,
– cracking and redistribution effects,
– properties of specific materials like reinforced, prestressed, high-strength, fibre reinforced [7] and textile-reinforced concrete [8, 9],
– geometrical characteristics like specific section shapes or complicated structural nodes,
– loading characteristics like static, fatigue or impact loading or constraint conditions,
– lifetime evaluations [10],
– multi-scale approaches from micro to meso and macro scales [11, 12].

Received March 2010

The core element of all numerical considerations is the material model of concrete. It is often formulated in the framework of elasto-plastic damage theories for continuous bodies to derive damaging effects of cracking from plastic strains. Thus, cracks are phenomenologically treated and "smeared" over element lengths.

In the paper, a computational modelling approach is presented using the example of RC shear beam tests. The basic aspects are revealed and typical numerical results are illustrated and compared to experimental data. Figure 1 shows the experimental setup of a three-point-bending test, where the attribute of specific interest is the circular shape of the section. Two experiments A1 and A4 are chosen out of a total series performed at the Ruhr-University of Bochum [13]. They only differ in their amounts of stirrups, namely – in case A1 – no stirrups (despite the regions of load application and bearing) to achieve a brittle shear failure by inclined concrete cracking and – in case A4 – a moderate and regular number of stirrups to gain ductile shear failure modes introduced by stirrup yielding.

No.	section	sideview	material properties	
			concrete	reinforcement
A1	D = 400 mm 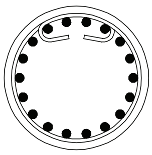	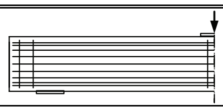	$f_{c,cyl}$ = 25,12 f_{ct} = 2,59 E_c = 34232 [MPa]	(long. / transv.) f_y = 529,0 / 618,4 f_t = 641,1 / 669,7 E_s = 197856 / 205882 [MPa]
A4	18 Ø 25	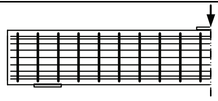 Ø 10 - 150 mm		

Fig. 1 Shear tests of RC members with circular cross sections [13]

2. Numerical Simulations

The major advantages of numerical investigations are their variability and effectiveness compared to elaborate experiments – however, experiments are still indispensable for principle verifications. Consequently, the finite element model is build up in a parametric way to allow for easy variations in basic parameters like reinforcement geometries and amounts, material parameters or section and length sizes.

2.1 Finite element model

Figure 2 shows the parametric finite element model of a typical three-point-bending test, where the specific section and thus the shape of the stirrups are of circular shape. It takes advantage of the symmetries in geometry and load and discretely models each circumferentially arranged longitudinal bar and each stirrup by a number of isoparametric spatial truss elements. The elements are embedded in the concrete volume and coupled to the linear 8-node solids with no additional slip conditions. Nonlinear springs prevent unrealistic tensile stresses at the edge of the support.

2.2 Material model for concrete

An elasto-plastic damage model is used to describe the nonlinear material properties of concrete [14-16]. It bases on the classical continuum damage theory [4] assuming geometric linearity. The model was developed by Lubliner, Oliver, Oller & Onate [17, 18] and elaborated by Lee & Fenves [19].

2.2.1 *Basic Equations*

Starting from an additive strain rate decomposition in elastic and plastic parts

$$\dot{\boldsymbol{\varepsilon}} = \dot{\boldsymbol{\varepsilon}}^{el} + \dot{\boldsymbol{\varepsilon}}^{pl} \tag{1}$$

the stress-strain relation is given in a matrix form by

$$\boldsymbol{\sigma} = (1-d)\mathbf{D}_0(\boldsymbol{\varepsilon} - \boldsymbol{\varepsilon}^{pl}), \tag{2}$$

where d with $0 \leq d < 1$ is a scalar damage variable and the matrix $\mathbf{D}_0$ contains the initial, elastic material properties. So, isotropic reductions of stiffness $\mathbf{D} = (1 - d)\mathbf{D}_0$ model cracking. Similar, effective values of stresses $\overline{\boldsymbol{\sigma}}$ are introduced by $\boldsymbol{\sigma} = (1-d)\overline{\boldsymbol{\sigma}}$. A yield function F of combined (modified) Drucker-Prager and Rankine type determines states of failure or damage.

$$F = F(\overline{\boldsymbol{\sigma}}, \tilde{\boldsymbol{\varepsilon}}^{pl}) = \frac{1}{1-\alpha}(\overline{q} - 3\alpha\overline{p} + \beta(\tilde{\boldsymbol{\varepsilon}}^{pl})\langle\overline{\sigma}_{\max}\rangle - \gamma\langle-\overline{\sigma}_{\max}\rangle) - \overline{\sigma}_c(\varepsilon_c^{pl}) \tag{3}$$

with: $\tilde{\boldsymbol{\varepsilon}}^{pl} = (\varepsilon_t^{pl} \quad \varepsilon_c^{pl})^{\mathrm{T}}$, $\langle x\rangle = ½(x + |x|)$

It represents a surface in the effective stress space and depends on two hardening variables ε_t^{pl}, ε_c^{pl}, the hydrostatic pressure $p = -I_1/3$ and the von Mises equivalent stress $q = (3J_2)^{1/2}$. α, $\gamma = 3$ [14, 17] and β denote material parameters and a material function, respectively. They include the ratio α_f of the biaxial to the uniaxial compressive strength.

$$\alpha = \frac{\alpha_f - 1}{2\alpha_f - 1}, \quad 0 \leq \alpha < 0{,}5 \tag{4}$$

$$\beta = \frac{\overline{\sigma}_c(\varepsilon_c^{pl})}{\overline{\sigma}_t(\varepsilon_t^{pl})}(1-\alpha) - (1+\alpha) \tag{5}$$

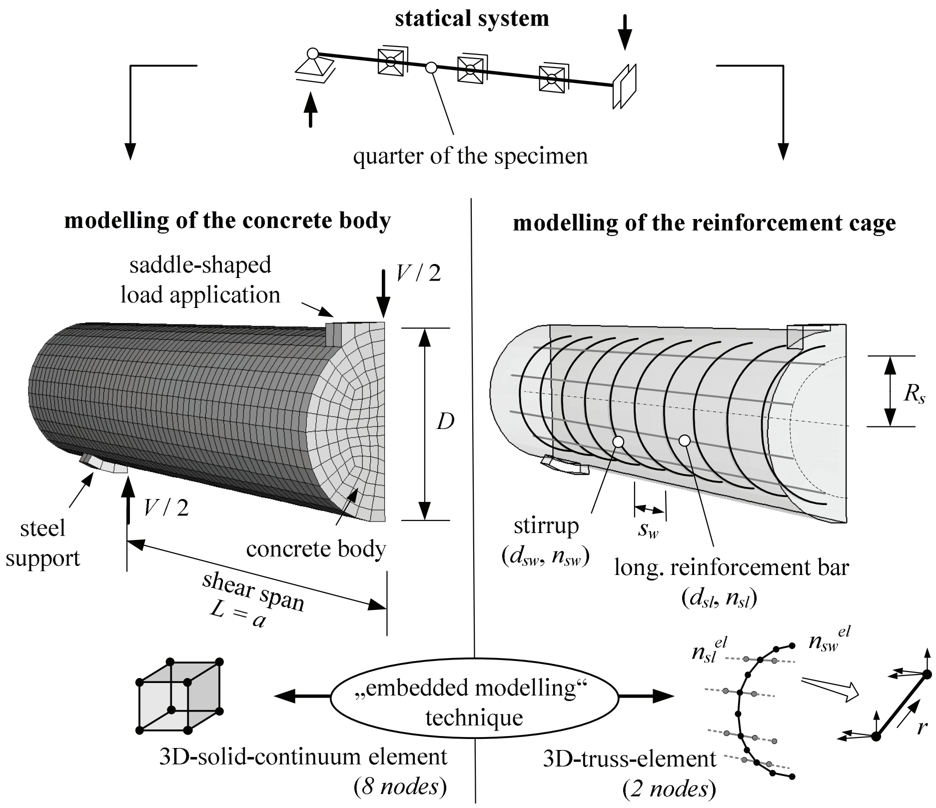

Fig. 2 Finite element model and parameters

The evolution of the hardening variables is linked to the three eigenvalues $\dot{\varepsilon}_1^{pl} \geq \dot{\varepsilon}_2^{pl} \geq \dot{\varepsilon}_3^{pl}$ in $\dot{\hat{\boldsymbol{\varepsilon}}}^{pl}$ of the plastic strain rate tensor

$$\dot{\tilde{\boldsymbol{\varepsilon}}}^{pl} = \begin{bmatrix} r(\hat{\bar{\boldsymbol{\sigma}}}) & 0 & 0 \\ 0 & 0 & r(\hat{\bar{\boldsymbol{\sigma}}})-1 \end{bmatrix} \dot{\hat{\boldsymbol{\varepsilon}}}^{pl} \tag{6}$$

via a multiaxial, principal stress condition

$$r(\hat{\bar{\boldsymbol{\sigma}}}) = \begin{cases} \dfrac{\sum_{i=1}^{3} \langle \bar{\sigma}_i \rangle}{\sum_{i=1}^{3} |\bar{\sigma}_i|}, & \bar{\boldsymbol{\sigma}} \neq \mathbf{0} \\ 0 \qquad , & \bar{\boldsymbol{\sigma}} = \mathbf{0} \end{cases} \tag{7}$$

that controls the distributions on ε_t^{pl} and ε_c^{pl}. Consistently, only ε_t^{pl} or ε_c^{pl} are activated in cases of uniaxial tensile or compressive loading.

Plastic flow is governed by the plastic flow potential G according to the non-associated flow rule

$$\dot{\boldsymbol{\varepsilon}}^{pl} = \dot{\lambda}\frac{\partial G(\overline{\boldsymbol{\sigma}})}{\partial \overline{\boldsymbol{\sigma}}}, \tag{8}$$

where G is of modified Drucker-Prager type and formulated in the plane of the effective values of p and q.

$$G = -\overline{p}\tan\psi + \sqrt{(\alpha_e f_{ct}\tan\psi)^2 + \overline{q}^2} \tag{9}$$

ψ, f_{ct}, $\alpha_e \geq 0$ denote the dilation angle, the tensile concrete strength and a material parameter α_e that affects the exponential deviation of G from the linear Drucker-Prager flow potential, especially for small confining pressures.

Figure 3 illustrates that strength results obtained from the material model – no matter of being under uniaxial, biaxial or triaxial loading conditions – agree well with experimental data taken from the literature. The comparisons are related to average values of the compressive strength f_c and summarised in the plane of p and q.

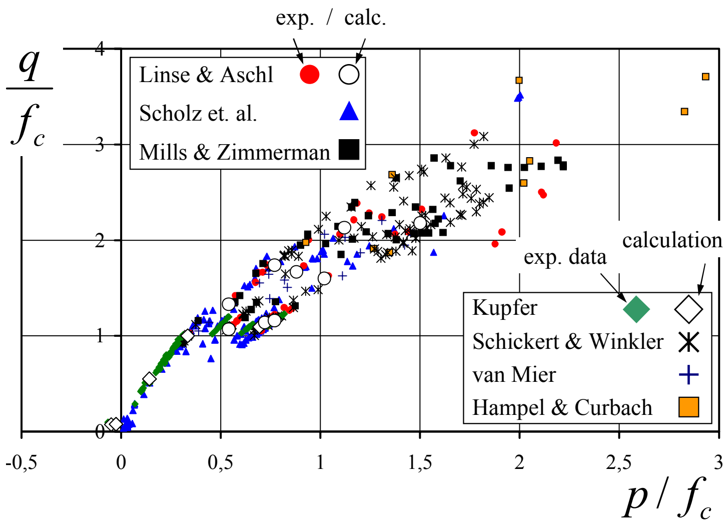

Fig. 3 Uniaxial, biaxial and triaxial strength results in the plane of p and q compared to experimental data

Damage is caused by cracking or crushing under tensile or compressive loading conditions. Thus, tensile d_t as well as compressive d_c parts constitute the total damage d

$$1 - d = (1 - s_c d_t)(1 - s_t d_c), \tag{10}$$

where the two functions s_t, s_c add in stiffness effects arising from closing and reopening of cracks.

$$s_t = 1 - \tfrac{1}{2} r(\hat{\boldsymbol{\sigma}}) \qquad s_c = r(\hat{\boldsymbol{\sigma}}) \tag{11}$$

A complete recovery of stiffness is assumed for crack closing and a partial transference of damage d_c takes place in cases of load cycles from compression to tension (factor ½). Figure 4 illustrates the assumptions for a cyclic, uniaxial loading path from tensile to compressive loading and back to the tensile side. Unloading occurs linearly and plastic concrete strains remain for $\sigma = 0$.

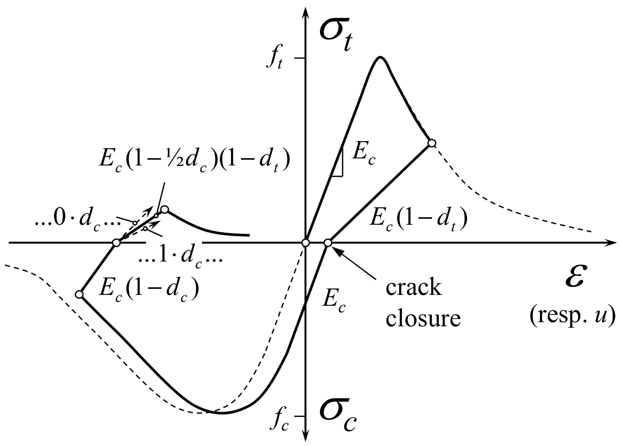

Fig. 4 Uniaxial loading path with stiffness recovery

2.2.2 Material equations and parameters

Three stepwise defined material functions describe the stress-strain behaviour under monotonic, uniaxial compressive loading (Figure 5).

$$\sigma_{c(1)} = E_c \varepsilon_c \tag{12}$$

$$\sigma_{c(2)} = \frac{E_{ci} \dfrac{\varepsilon_c}{f_{cm}} - (\varepsilon_c / \varepsilon_{c1})^2}{1 + (E_{ci} \dfrac{\varepsilon_{c1}}{f_{cm}} - 2) \dfrac{\varepsilon_c}{\varepsilon_{c1}}} f_{cm} \tag{13}$$

$$\sigma_{c(3)} = \left(\frac{2 + \gamma_c f_{cm} \varepsilon_{c1}}{2 f_{cm}} - \gamma_c \varepsilon_c + \frac{\gamma_c \varepsilon_c^2}{2 \varepsilon_{c1}} \right)^{-1} \tag{14}$$

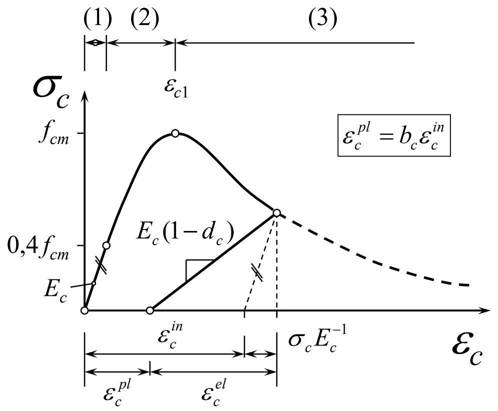

Fig. 5 Stress-strain relation and linear unloading path (compressive loading)

They are derived from the recommendations of the Model Code 1990 [20], slightly modified in the slope parameter E_{ci} of the ascending branch and elaborated for the descending branch [21] to take account for its dependency on the specimen geometry [22, 23]. There, a function $\gamma_c > 0$ controls the descent, incorporating the ratio G_{cl}/l_c of the crushing energy and an internal length parameter to achieve almost mesh independent results of simulations. Unloading occurs linear elastically with the degraded modulus of elasticity. The evolution of damage d_c is linked to the plastic strain ε_c^{pl} which is determined proportional to the inelastic strain $\varepsilon_c^{in} = \varepsilon_c - \sigma_c E_c^{-1}$ using a constant factor b_c with $0 < b_c \leq 1$. A value $b_c = 0{,}7$ fits well with experimental data of cyclic tests [24], so most of the inelastic compressive strain is retained after unloading.

$$d_c = 1 - \frac{\sigma_c E_c^{-1}}{\varepsilon_c^{pl}(1/b_c - 1) + \sigma_c E_c^{-1}} \tag{15}$$

The simplified material equation for uniaxial tensile loading bases on the "Fictitious Crack Model" of Hillerborg [25]. It is subdivided into two parts. First, loading up to the strength f_{ct} occurs linearly. The second, descending branch arises from the stress-crack opening relation of Hordijk [26] (Figure 6):

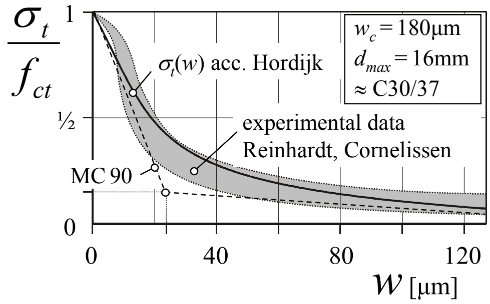

Fig. 6 Stress-crack opening relation [26] compared to experimental data [27]

$$\frac{\sigma_t(w)}{f_{ct}} = [1 + (c_1 w / w_c)^3]\ e^{-c_2 \frac{w}{w_c}} - \frac{w}{w_c}(1 + c_1^3)e^{-c_2}\ , \tag{16}$$

where $c_1 = 3$, $c_2 = 6{,}93$ and a product of inelastic strain and length parameter l_t replaces the crack opening w to yield $\sigma_t = \sigma_t(w = l_t \varepsilon_t^{in})$ with $\varepsilon_t^{in} = \varepsilon_t - \sigma_c E_c^{-1}$. So w is smeared over the average element length $l_t = V_e^{1/3}$ and $\sigma_t(\varepsilon_t)$ encloses G_F/l_t. Similar to (15) the damage d_t depends on ε_t^{pl} and an experimentally determined parameter $b_t = 0{,}1$. So, unloading returns almost back to the origin and leaves only a small residual strain.

$$d_t = 1 - \frac{\sigma_t E_c^{-1}}{\varepsilon_t^{pl}(1/b_t - 1) + \sigma_t E_c^{-1}} \tag{17}$$

Table 1 summarises the material parameters of the model.

Table 1 Material parameters

Parameter	Denotation
uniaxial loading	
$E_c = E_{cm}, f_{cm}, f_{ctm}$ $b_c = 0.7$, $b_t = 0.1$ $G_F = 0{,}195 w_c f_{ctm}$, $G_{cl} = 15$kN/m [23] $w_c = 180\mu$m, $\varepsilon_{c1} = -2{,}2‰$	acc. Eurocode 2 [28] and experimental data damage parameters, ($0 < b_c, b_t \leq 1$) [21] fracture and crushing energies max. crack opening [26], strain at f_{cm} [20]
multiaxial loading	
$\nu = 0{,}2$ $\psi = 30°$ $\alpha_f = 1{,}16 \quad (\rightarrow \alpha = 0{,}12)$ $\alpha_e = 0{,}1$	Poisson's ratio dilation angle [19] ratio of biaxial to uniaxial compressive strength [29] parameter of the flow potential G

2.3 Results

Figures 7 and 8 represent typical numerical results compared to experimental data, namely overall load-deflection curves and corresponding damage evolutions illustrated by the distributions of the plastic strains and experimental crack patterns at the lateral surfaces of the concrete body. The overall load-deflection curves prove good correspondences to the brittle failure characteristic in case A1 – the numerically evaluated graph even exhibits a little snap-back effect – and in the second case A4, where a pronounced yielding plateau with redistributions in strut-and-tie mechanisms occur. Shear cracks develop after a first damage stage dominated by bending with almost vertical crack orientations. In case of A1, plastic strains localise into one single inclined crack governing the failure. On the contrary (A4), the stirrups hang back the diagonal compressive shear struts into the compressive zone and spread stresses and cracking. A behaviour of designated ductile and deformable nature arises.

Figure 9 offers a view inside the concrete body (A4) that only simulations are able to give. On the one hand, it displays the principle compressive concrete stresses at peak load. They already form a pattern of inclined struts separated by diagonal shear cracks. On the other hand, it visualises the distribution of the stresses in the stirrups and their evolution over the loading process. After shear cracking – occurring here at about 3mm of deflection in midspan – the circular stirrups start acting like rings under internal pressures and thus obtain almost uniform stresses [13, 16]. Simulation and experiment evidently correspond well in their developments despite a little quantitative underestimation of the total stress extents of about 10 to 20%. This matches well with the underestimating approximation of the overall shear bearing capacity (cp. Figure 7) in cases of ductile behaviours that require pronounced redistributions onto the stirrups.

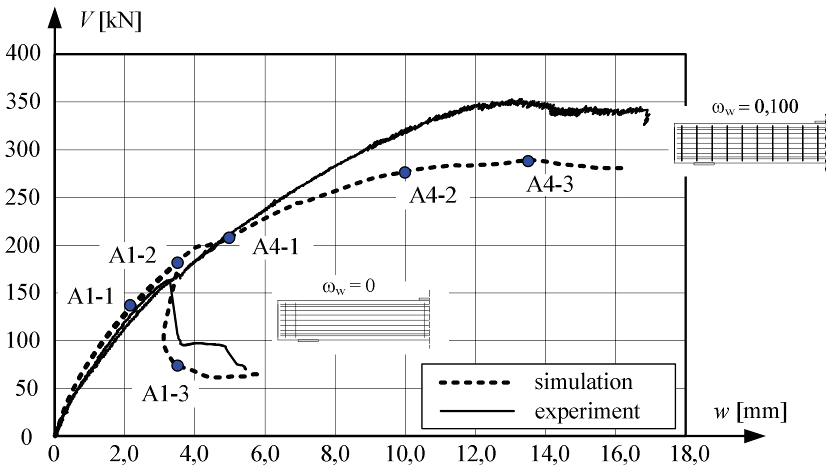

Fig. 7 Comparison of experimental and calculated load deflection curves

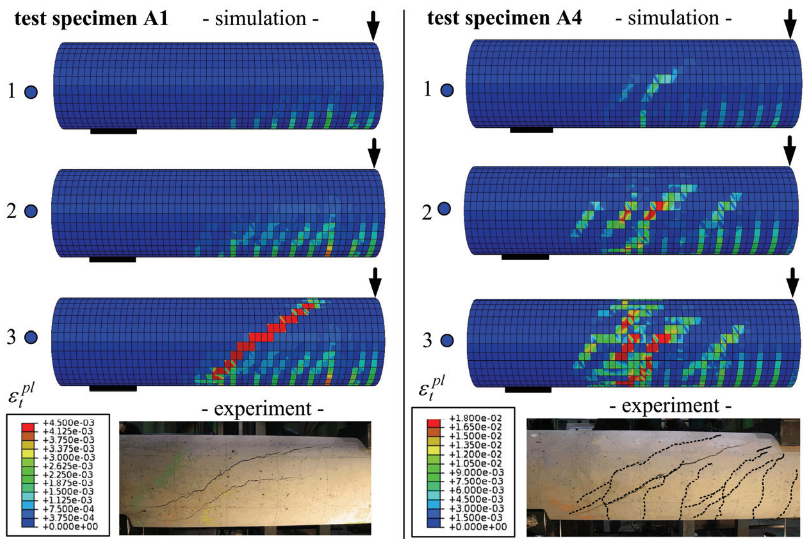

Fig. 8 Evolution of plastic tensile strains with increasing load and experimental crack patterns, left: brittle bearing behaviour (A1), right: ductile bearing behaviour (A4)

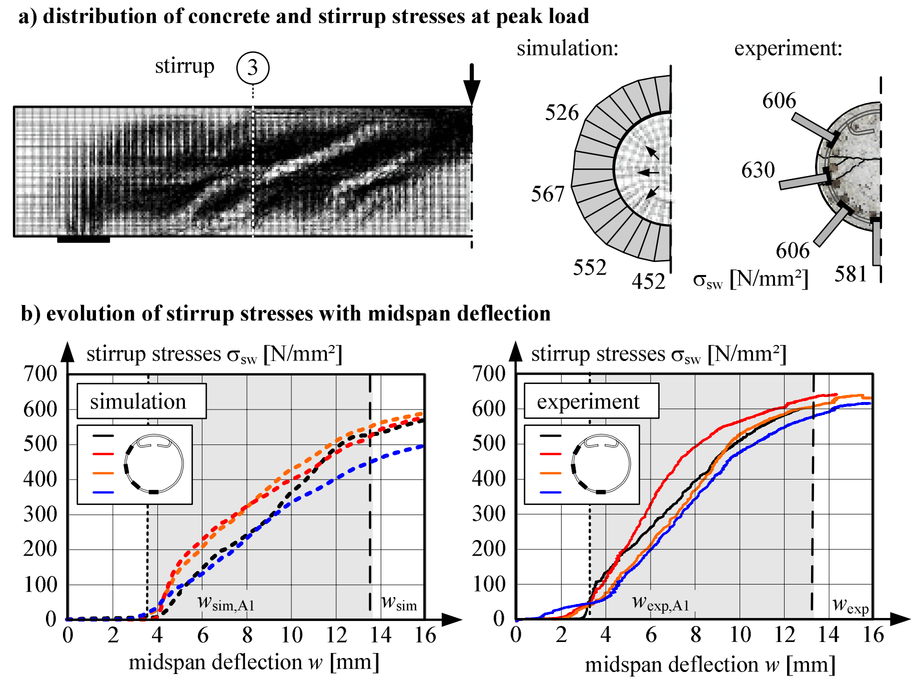

Fig. 9 Calculated concrete and stirrup stresses and comparison to experimental data (test specimen A4, stirrup 3)

3 CONCLUDING REMARKS

Numerical simulations with parametric finite element models are powerful and robust tools for comprehensive investigations of bearing capacities and failure mechanisms of reinforced concrete structures. They reliably evaluate global parameters, like ultimate loads and deflections, close to reality and easily allow extended parameter variations that experiments – due to their demand on time and costs – are not able to give. Moreover, simulations open the view to the inside of structures. Stresses and strains can be monitored not only point wise – e.g. by strain gauges –, but in their overall spatial distributions and developments over loading histories to properly understand inner bearing and redistribution mechanisms. Consequently, nonlinear calculations are applied more and more in design processes of complex structural elements.

However, experiments and numerical investigations have to go hand in hand. Experimental verifications of basic numerical data are still indispensible to insure reliable numerical results.

REFERENCES

1. G. Meschke, et al. (eds): *Computational Modelling of Concrete Structures*, Proceedings of EURO-C 2006, Taylor & Francis, 2006, London.
2. A. Carpinteri, et al. (eds): *Fracture Mechanics of Concrete and Concrete Structures*, Proceedings of FraMCoS-6, Taylor & Francis, 2007, London.
3. J. Lemaitre, J.-L. Chaboche: *Mechanics of solid materials*, Cambridge University Press, 1990, Cambridge.
4. L.M. Kachanov: *Introduction to Continuum Damage Mechanics*, Kluwer Academic Publisher, 1990, Dordrecht.
5. K.-J. Bathe: *Finite Element procedures,* Prentice Hall, 1996, New Jersey.
6. O.C. Zienkiewicz, R.L. Taylor: *The finite element method*, Butterworth-Heinemann, 2000, Oxford.
7. L. Gödde, M. Strack: *Residual-strength-dependent conversion factors for the determination of the tensile behaviour of steel fibre reinforced concrete by bending tests*, Proc. of the 7th RILEM International Symposium (BEFIB 2008) Fibre Reinforced Concrete: Design and Applications, 2008, India, 409-418.
8. J. Hartig, U. Häußler-Combe: *A model for Textile Reinforced Concrete exposed to uniaxial tensile loading,* Proc. of the 18th Int. Conf. on Computer Methods in Mechanics (CMM2009), The University of Zielona Góra Press, 2009, 203-204.
9. R. Ortlepp, F. Schalditz, M. Curbach: *TRC-Strengthening for Normal and Torsion Loads*, Proc. of the 18th Int. Conf. on Computer Methods in Mechanics (CMM2009), The University of Zielona Góra Press, 2009, 345-346.
10. F. Stangenberg, et al. (eds): *Lifetime-Oriented Structural Design Concepts*, Springer-Verlag, 2009, Berlin.
11. Z.P. Bazant, J. Planas: *Fracture and size effect in concrete and other quasibrittle materials*, CRC Press LLC, 1989, Florida, USA.
12. O.T. Bruhns, G. Meschke: *Deterioration of Materials and Structures: Phenomena, Experiments and Modelling*, In F. Stangenberg, et al. (eds): Lifetime-Oriented Structural Design Concepts, Springer-Verlag, 2009, Berlin.
13. M. Bender: *Shear design of RC girders with circular sections*, PhD-thesis, 2010, Ruhr-University Bochum.
14. ABAQUS: *Theory Manual (Version 6.8)*, ABAQUS Inc., 2008, USA.
15. P. Mark: *Investigations of reinforced concrete girders under biaxial shear using parametric finite element models*, Computational modelling of concrete structures (EURO-C 2006), Taylor & Francis/Balkema, 2006, Leiden, 739 - 746.
16. M. Bender, P. Mark: *Shear Bearing Capacities of RC Beams with Circular Sections: Computational Modelling and Design*, Proc. of the Eighth International Conference on Computational Structures Technology (CST 2006), Civil-Comp Press, 2006, Scotland, 289 - 290 (CD-Rom).
17. J. Lubliner, J. Oliver, S. Oller, E. Onate: *A plastic-damage model for concrete*, Int. J. Solids Structures 25(3), 1989, 299-326.
18. S. Oller, E. Onate, J. Oliver, J. Lubliner: *Finite element nonlinear analysis of concrete structures using a "plastic-damage model"*, Engineering Fracture Mechanics 35(1/2/3), 1990, 219-231.
19. J. Lee, G.L. Fenves: *Plastic-damage model for cyclic loading of concrete structures*, J. Eng. Mechanics 124(8), 1998, 892-900.
20. CEB-FIP: *Model Code 1990*, Thomas Telford, 1993, London.
21. W.B. Krätzig, R. Pölling: *An elasto-plastic damage model for reinforced concrete with minimum number of material parameters*, Computers and Structures 82, 2004, 1201-1215.
22. J.G.M. van Mier: *Strain-softening of concrete under multiaxial loading conditions*, PhD-Thesis, 1984, TU Eindhoven.
23. R.A. Vonk: *A micromechanical investigation of softening of concrete loaded in compression*, Heron 38(3), 1993, 3-94.
24. B.P. Sinha, K.H. Gerstle, L.G. Tulin, L.G.: *Stress-strain relations for concrete under cyclic loading*. Journal of the ACI 61(2), 1964, 195-211.
25. A. Hillerborg: *Analysis of one single crack*, Fracture mechanics of concrete, Elsevier, 1983, Amsterdam, 223-249.
26. D.A. Hordijk: *Tensile and tensile fatigue behaviour of concrete - experiments, modelling and analyses*, Heron 37(1), 1992, 3-79.

27. H.W. Reinhardt, H.A.W. Cornelissen: *Post-peak cyclic behaviour of concrete in uniaxial tensile and alternating tensile and compressive loading*, Cement and Concrete Research 14(2), 1984, 263-270.
28. Eurocode 2-1-1: *Design of concrete structures - Part 1-1: General rules and rules for buildings*, 2004.
29. H.B. Kupfer, K.H. Gerstle: *Behaviour of concrete under biaxial stresses*, Journal of the Engineering Mechanics Division 99(EM4), 1973, 853-866.

NUMERIČKO MODELOVANJE MEHANIZMA LOMA U ARMIRANO-BETONSKIM KONSTRUKCIJAMA

Peter Mark, Michél Bender

U radu je izložen jedan pristup numeričkom modeliranju armirano-betonskih konstrukcija i konstrukcijskih elemenata pod statičkim opterećenjem. Korišćena je tehnika unutrašnjeg modeliranja koja odvojeno tretira betonski deo preseka, podužnu i poprečnu armaturu. Jednačine kojima se opisuje prostorni elastoplastični model loma za beton, izvedene su pod pretpostavkom izotropnog loma i reverzibilne krutosti usled povećanja i smanjenja otvora prslina. Date su odgovarajuće funkcije ponašanja materijala i odgovarajući parametri, bazirani na kriterijumu održanja energije. Numerički model je verifikovan eksperimentalnim ispitivanjem grede izložene smicanju i upoređivanjem numeričkih i eksperimentalnih rezultata.

Ključne reči: *numerička simulacija, armirani beton, model betona, unutrašnje modeliranje, razvoj loma, lom usled smicanja, kružni poprečni presek*